Ab initio study on fcc Pr with correlation matrix renormalization theory

Jun Liu,[1] Yongxin Yao,[1,2] Jianhua Zhang,[2,3] Vladimir Antropov,[1,2] Kai-Ming Ho,[1,2] and Cai-Zhuang Wang[1,2,*]

[1]*Ames Laboratory–USDOE, Iowa State University, Ames, Iowa 50011, USA*

[2]*Department of Physics and Astronomy, Iowa State University, Ames, Iowa 50011, USA*

[3]*Department of Physics, Hainan University, Haikou 570228, China*

(Received 21 August 2022; revised 29 September 2022; accepted 24 October 2022; published 15 November 2022)

We studied fcc praseodymium (Pr) with the *ab initio* correlation matrix renormalization theory (CMRT) explicitly calculating the Coulomb interactions among basis orbitals and without using any adjustable parameters to work for strongly correlated electron systems. We calculated its total energy in a paramagnetic ground state and studied the role of the correlated $4f$ electrons in the system. Good agreement was obtained between CMRT and experiments in the pressure volume dependence of the fcc phase. We also compared the CMRT results against other theoretical methods including local density approximation+dynamical mean-field theory and showed consistent results among them. Moreover, we found the normalized local charge fluctuation of the $4f$ electrons as the function of volume exhibits a clear slope change at the volume collapse region, indicating a switch in their correlation nature there.

DOI: 10.1103/PhysRevB.106.205124

I. INTRODUCTION

Electron correlation plays a critical role in governing many important properties of materials (i.e., superconductivity, magnetism, quantum coherences, etc.) for clean energy applications and advanced technologies. However, accurate and efficient calculations and predictions of materials stability and properties with the presence of strong electron correlations have been a long-standing challenge. First-principles density-functional theory (DFT) based on the Kohn-Sham approach [1,2] has achieved significant success for weakly correlated materials, but it is not adequate for systems with strong correlation, especially for rare-earth materials containing partially filled $4f$ electron shells [3]. To go beyond DFT, many computational methods have been explored. While *ab initio* methods such as quantum Monte Carlo (QMC) [4,5]or wave function-based quantum chemistry methods and their improvements with density-matrix renormalization group (DMRG) [6,7] or quantum embedding [8,9] techniques can be accurate, the computational workload in some of these methods remains very heavy, and the application to real $4f$ rare-earth (RE) materials is limited. Hybrid approaches merging DFT with many-body techniques for improved treatment on local correlations have also been developed, including DFT+Hubbard U (DFT+U) [10,11], DFT+dynamical mean-field theory (DFT+DMFT) [12], and DFT+Gutzwiller approximation (DFT+G) [13–15]. These methods are faced with limitations of exploiting empirical screened Hubbard U and exchange J parameters [16] and multiple choices of double-counting corrections [17,18], both of which weaken their predictive powers. Therefore, robust *ab initio* theories and computational methods with accurate and efficient predictive power for real correlated materials are still lacking and highly desired.

Recently, we have been tackling this grand challenge problem through the development of a fully *ab initio* correlation matrix renormalization theory (CMRT) [19–21] with a computational workload similar to minimum basis Hartree-Fock (HF) calculations. We have shown reasonable performance of CMRT in both weakly and strongly correlated electron systems [21,22]. We now apply CMRT to fcc praseodymium (Pr) to demonstrate its performance against experiments and other computational methods. As a rare-earth element, Pr is believed to have its physical properties affected by the strongly correlated $4f$ electrons [3]. Pr has a divalent electronic configuration, $[\mathrm{Xe}]4f^{3}6s^{2}$, as a free atom and becomes trivalent, $[\mathrm{Xe}]4f^{2}5d^{1}6s^{2}$, in a lattice environment. The change results from a competition between energy cost to excite one $4f$ electron to the $5d$ state and cohesive energy gain of this electron to participate in bonding and forming lattice [23]. Pr exhibits polymorphism under temperature and pressure [24]. At ambient temperature, Pr undergoes a series of phase transitions with pressure: Pr-I(dhcp) at ambient pressure $\rightarrow$ Pr-II(fcc) $\rightarrow$ Pr-III[distorted fcc(dfcc)] $\rightarrow$ Pr-IV(α-U) as the pressure increases, accompanied with a sizable volume collapse (about 10%) between Pr-III and Pr-IV which is interpreted to be due to $4f$ electron delocalization [25]. The density of states (DOS) of dhcp Pr was measured with high-energy spectroscopies such as x-ray photoelectron spectroscopy (XPS) and bremsstrahlung isochromat spectroscopy (BIS) where the lower and upper Hubbard peaks are easily seen [26,27].

Structural properties of Pr have been studied for a long time using a large variety of electronic structure methods. DFT with local density approximation (LDA) was applied to fcc Pr and produced a tentative band structure, Fermi surface, and magnetic susceptibility [28] as well as too small equilibrium volumes [29] while DFT with the generalized gradient approximation (GGA) only mildly improves on LDA. A major

*Corresponding author: wangcz@ameslab.gov

concern of DFT towards Pr is the excessive DOS, presumably of $4f$ character, at the Fermi level as compared with experimental data inferred from specific-heat measurement [30]. Consequently, any additional treatment which helps removing $4f$ states from the Fermi level would be a reasonable approach towards improving agreement between theory and experiment. One way to do so is to add spin polarization plus spin-orbit coupling (SOC) to GGA and much better cohesive properties were rendered, including both equilibrium volume and bulk modulus, towards fcc Pr [31]. Another way is to introduce additional components to DFT targeting the localized $4f$ electrons. The so-called "standard model" towards RE elements (fcore-DFT) goes one step further beyond DFT by including $4f$ electrons into core electrons thus excluding them from hybridization with valence electrons nor the formation of chemical bonds [29,32]. Such a simple treatment greatly improves the predictions of DFT in physical quantities ranging from cohesive to PES and BIS excited-state properties albeit outlying performance on light lanthanide including Pr, confirming the localized nature of $4f$ electrons at the equilibrium lattice structures of RE [29,32,33]. However, including $4f$ electrons into core electrons is ad hoc and does not always have better results. For example, the volume collapse transition of Pr captured by the spin-polarized GGA calculation is missed in the standard model of RE elements [29]. Other localization-treating enhancements of DFT include adding orbital polarization (DFT-OP) or self-interaction correction (SIC-DFT) terms to DFT [34–36]. They were able to produce the needed localization of $4f$ electrons and the accompanying local moments by the localization enforcement within their formalism [34,37], successfully reduce number of $4f$ electrons at the Fermi level [37], and produce comparable cohesive properties as the standard model of REs. Meanwhile, both DFT-OP and SIC-DFT produced the expected volume-collapse transition [36]. It is worth mentioning a hybrid DFT calculation, HSE06, on fcc Pr treated all electrons as being band-like but rendered very good cohesive properties regardless of spin polarization [38].

While the localization-enforced DFT methods and the standard model for RE mentioned above could successfully produce some properties of the rare-earth material, these methods pre-assume or produce a rather abrupt delocalization of the $4f$ electrons likely originated from their static mean-field nature [39]. While there are ways to get excitation energies of the XPSand BIS processes, these methods fail to produce the details of the XPS and BIS spectra due to lack of accurate description of strong correlation effect of $4f$ electrons. Also, the mean-field nature of these methods causes difficulty in reproducing measured multiplet features and magnetic properties expected from a Russel-Saunders ground state [40]. All these concerns can in principle be properly addressed by carefully treating the local correlation effects, as done in DFT embedding theories including LDA+DMFT and LDA+G methods. They explicitly incorporate a local many-body Hamiltonian in the correlated $4f$ subspace to help capture these effects and were both applied to the Pr phases. Scattered in several separate research works with different technical choices of impurity solver and double-counting term, LDA+DMFT is capable of giving a plethora of physical quantities ranging from cohesive properties to local spin and charge properties and to spectral functions at finite temperature [39–41]. Good agreement was achieved between theory and experiment [40], giving solid evidence on the overall validity of this method towards Pr as well as other RE materials. LDA+G, on the other hand, was able to compute volume dependence of the total energy of both fcc and α-U phases and correctly captured the volume collapse transition between the two phases [15]. However, the model-related U, J parameters and choices of double-counting terms [40] limit their predictive power.

The above-mentioned methods suffer from artificial localization enforcement in the modified DFT methods or the standard model of REs, ad hoc mixing parameters in the hybrid DFT, adjustable energy parameters, and double-counting issues in LDA+DMFT and LDA+G, not to mention the self-interaction issue in DFT itself. None of these exist in the CMRT method, being a fully *ab initio* method working directly with real Coulomb interactions [20,21,42]. Furthermore, CMRT intrinsically includes local spin and charge fluctuation effects in its formalism and preserves local moment physics. It is capable of describing similar physics as LDA+DMFT as far as their theoretical descriptions are concerned. In this work, we will perform the CMRT calculation on fcc Pr in a paramagnetic ground state and compare it with LDA+DMFT as well as other methods. We will discuss producing the experimental pressure volume curve, calculating the local $4f$ occupational probability and its local charge-fluctuation effect.

II. METHODS

CMRT is a fully *ab initio* variational theory specifically designed for strongly correlated electron systems by taking a multiband Gutzwiller wave function as its trial wave function [21]. For a periodic bulk system with one atom per unit cell in a paramagnetic state, the CMRT ground-state total energy is

$$E_{total} = \sum_{\substack{ij \\ \alpha\beta,\sigma}} t_{i\alpha,j\beta}\langle c^{\dagger}_{i\alpha\sigma} c_{j\beta\sigma}\rangle + \frac{1}{2}\sum_{\substack{ijkl \\ \alpha\beta\gamma\delta,\sigma\sigma'}} \left(U^{\alpha\beta\gamma\delta}_{ijkl} - \lambda^{\alpha\beta\gamma\delta}_{ijkl}\right)\left(\langle c^{\dagger}_{i\alpha\sigma} c_{k\gamma\sigma}\rangle\langle c^{\dagger}_{j\beta\sigma'} c_{l\delta\sigma'}\rangle - \delta_{\sigma\sigma'}\langle c^{\dagger}_{i\alpha\sigma} c_{l\delta\sigma'}\rangle\langle c^{\dagger}_{j\beta\sigma'} c_{k\gamma\sigma}\rangle\right) + \sum_{i}\sum_{\Gamma} E_{i\Gamma}(p_{i\Gamma} - p_{i\Gamma_0}), \tag{1}$$

with i, j, k, l for site indices, $\alpha, \beta, \gamma, \delta$ for orbital indices, σ, σ' for spin indices, and Γ labeling the Fock states in the occupation-number representation of local correlated orbitals (e.g., $4f$ orbitals in rare-earth systems). The energy

parameters, $t_{i\alpha,j\beta}$, $U_{ijkl}^{\alpha\beta\gamma\delta}$, and $E_{i\Gamma}$ represent bare hopping, bare Coulomb integrals, and eigenvalues of a bare local correlated Hamiltonian, respectively. Specifically, the local Coulomb integral is defined with the orbital basis set $\{\phi_{i\alpha}(\mathbf{r})\}$ as

$$U_{iiii}^{\alpha\beta\gamma\delta} = \int \phi_{i\alpha}^{*}(\mathbf{r})\phi_{i\beta}^{*}(\mathbf{r}')\frac{1}{|\mathbf{r}-\mathbf{r}'|}\phi_{i\gamma}(\mathbf{r})\phi_{i\delta}(\mathbf{r}')d\mathbf{r}d\mathbf{r}' \quad (2)$$

by taking the atomic units (a.u.) while the nonlocal $t_{i\alpha,j\beta}$ and $U_{ijkl}^{\alpha\beta\gamma\delta}$ are implicitly evaluated during code implementation. Note the orbital index convention, $U_{iiii}^{\alpha\beta\alpha\beta}$ is the energy coefficient of the two-body direct Coulomb interaction term of $\hat{n}_{i\alpha\sigma}\hat{n}_{i\beta\sigma'}$ in the second quantization.

The first two terms in Eq. (1) give the expectation value of the bare lattice Hamiltonian under the CMRT approximation, where the one-particle density matrix is evaluated as

$$\langle c_{i\alpha\sigma}^{\dagger}c_{i\beta\sigma}\rangle = f(z_{\alpha\sigma})f(z_{\beta\sigma})\langle c_{i\alpha\sigma}^{\dagger}c_{i\beta\sigma}\rangle_0 + [1-\delta_{\alpha\beta}f^2(z_{\alpha\sigma})]n_{i\alpha\sigma}^0. \quad (3)$$

Here, $z_{\alpha\sigma}$ is the Gutzwiller renormalization factor while $\langle\ldots\rangle_0$ is the one-particle noninteracting density matrix. $f(z_{\alpha\sigma})$ is introduced to ensure that CMRT reaches the solution of an exactly solvable model [20] at a certain limit. The third term in Eq. (1) serves the sole purpose of preserving dominant local physics in CMRT by rigorously evaluating the local correlated Hamiltonian in terms of $p_{i\Gamma}$ and $p_{i\Gamma_0}$ as true correlation-renormalized and noninteracting Fock state probabilities. In particular, this term helps preserve local spin and charge fluctuation effects and renders the local moment as needed. The sum-rule correction coefficients associated with the correlated orbitals, $\lambda_{ijkl}^{\alpha\beta\gamma\delta} = \lambda_i^{\alpha}\delta_{ik}\delta_{jl}(1-\delta_{ij})\delta_{\alpha\gamma}\delta_{\beta\delta}$, are uniquely introduced in CMRT to define a set of *null* sum rule Hamiltonians constructed on charge conservation and included in the bare lattice Hamiltonian. They are defined for a paramagnetic state in this work as [21]

$$\lambda_i^{\alpha} = -\sum_{j\neq i}\sum_{\beta}U_{ijij}^{\alpha\beta\alpha\beta}\left(\frac{|\langle c_{i\alpha,\sigma}^{\dagger}c_{j\beta,\sigma}\rangle|^4}{\sum_{j\neq i}\sum_{\beta}|\langle c_{i\alpha,\sigma}^{\dagger}c_{j\beta,\sigma}\rangle|^4}\right). \quad (4)$$

These sum-rule Hamiltonians help minimize error from the Fock terms in Eq. (1), a major error source of CMRT, and redistribute nonlocal Coulomb interactions to local sites to further improve accuracy. The variational process results in a Gutzwiller equation set whose solution is shown to be quantitatively comparable to experiments in weakly correlated lattice systems [21] and capable of capturing the correlated nature of $4f$ electrons in fcc Ce [22].

CMRT inherited from the Gutzwiller approximation (GA) [43,44] the central physical idea that the bare and correlated electronic motions are simply related through a renormalization prefactor. They differ in the following aspects. First, the renormalization prefactor towards each orbit is redressed with an extra function in CMRT to better capture correlation effects on total energy. Second, expectation values of generic two-body operators are disintegrated into one-body terms by adopting the Wick theorem, which better helps CMRT formulation as well as its speed. Third, a sum-rule correction term is included into CMRT to help reduce error coming from intersite direct Coulomb interactions, which are left untreated in GA. Last, CMRT is anchored against the exactly solvable model of a minimum basis hydrogen dimer to fix the theory for practical considerations. For more details please refer to Ref. [21].

To probe the local correlation physics and possible changes in the $4f$ electron's localization status, we have introduced the normalized local charge fluctuation (NLCF) for target electrons [22], defined as

$$\mathrm{NLCF} = \frac{\langle(\hat{n}-n)^2\rangle}{n^2} = \frac{\langle\hat{n}^2\rangle}{n^2} - 1, \quad (5)$$

with $\hat{n}$ being the number operator of the electrons of interest and n its expectation value. A simple derivation shows that it mainly varies as $1/n$ in the weak-interacting limit. With a decreasing charge occupation with lattice constant, it should show a bell shape which increases when the lattice constant is small and decays as the lattice constant further increases when electronic correlation gets stronger and local charge fluctuation gets increasingly suppressed. Both theoretical analysis and close connection with Ce's alpha and gamma phases [22] show the U-turn at the bell top necessarily indicates a delocalization-to-localization transition or crossover.

Interfaced with the Hartree-Fock (HF) module of the Vienna *Ab initio* Simulation Package (VASP) [45], CMRT is efficiently implemented with the quasi-atomic minimal basis set orbitals (QUAMBO) basis set [46] and has a computational speed of a minimal basis HF calculation [21,22], a great speed gain over quantum Monte Carlo methods. The calculations in this paper use a paramagnetic trial wave function to facilitate comparison with LDA+DMFT [39,41] and to check possible magnetic instability towards a magnetic state due to the Stoner mechanism. Brillouin-zone sampling is done by VASP with an automatically generated K-point grid taking a R_k length of 50 ($R_k = 50$). The total energy and local physical quantities agree very well with results from a smaller K-point grid of $R_k = 30$.

III. RESULTS

A. *E-V* and *P-V* curve comparisons among different methods and against experiments

Energy verses volume (E-V) curves in a paramagnetic ground state are collected and compared in Fig. 1, including LDA [15], GGA, LDA+DMFT [39], and CMRT for fcc Pr. Included also is a SIC-LSDA [36] energy curve typically chosen among the methods utilizing a spin-polarized ground state loaded with local moments. LDA and GGA are standard DFT calculations with all electrons treated as band-like. The figure also shows an inferred experimental E-V curve at $T = 632$ K [39], the same temperature at which LDA+DMFT was performed. The equilibrium volume and bulk modulus from each method are derived from the Birch-Murnaghan equation of state (BM-EOS) [47] fit on the energy volume data and are collected in Table I along with experiments. Taking the experimental equilibrium volume and bulk modulus as a reference, we can see a progressively improved performance in total energy from LDA to GGA to SIC-LSDA and then to LDA+DMFT as electronic correlation and local magnetic moment is more and more carefully treated. CMRT, on the other hand, makes correction on top of a Hartree-Fock Hamiltonian by incorporating nonlocal correlation effects

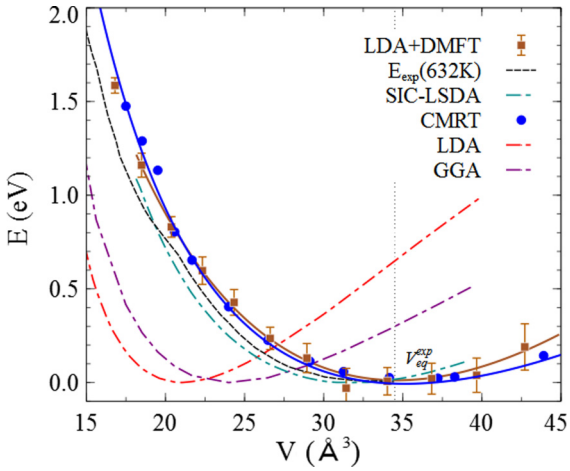

FIG. 1. E-V curves calculated with LDA [15], GGA, LDA + DMFT (U_f volume dependent, $T = 632$ K, with SOI) [39] and CMRT methods for fcc Pr in a paramagnetic ground state. SIC-LSDA [36] is included as a typical instance with a spin-polarized ground state. An experimental E-V curve at $T = 632$ K [39] is included and shown by the black dashed line. LDA, GGA, and SIC-LSDA are shown with dash-dotted lines. CMRT and LDA+DMFT are presented with dots while the lines are BM-EOS fit with respects to the dots. The reference experimental equilibrium volume per atom is taken from the thermodynamically stable dhcp phase of Pr [15]. All the energy curves are shifted to bring their lowest energies at 0 eV.

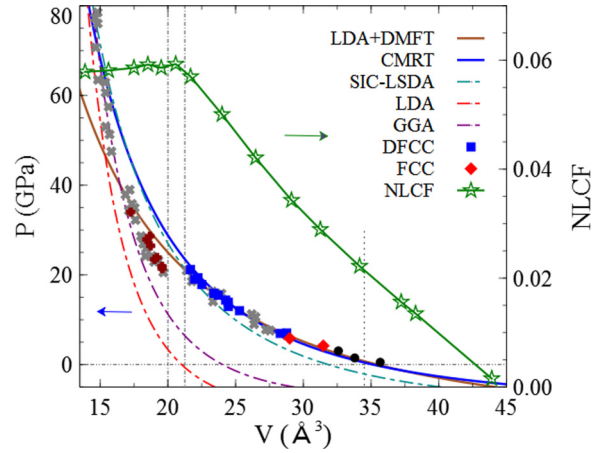

FIG. 2. The P-V curves fit from CMRT, LDA [15], GGA, SIC-LSDA [36], and LDA+DMFT (U_f volume dependent, $T = 632$ K, with SOI) [39] data on fcc Pr are compared against experiments [3,48]. LDA, GGA, and SIC-LSDA are shown by dash-dotted lines but in different colors while CMRT and LDA+DMFT are shown by blue and brown solid lines. One set of experimental measurements are shown as dfcc with blue squares, fcc with red diamonds, dhcp with black circles, α-U with brown plus signs [3]. The other set of experimental measurements are shown with gray crosses without phase identification [48]. Included also is the volume dependence of NLCF out of CMRT, shown with green stars linked with line segments. The two vertical gray dashed lines delineate the range of the experimental volume collapse transition. The horizontal dashed line represents zero pressure.

through dressed intersite hoppings plus accurate local onsite correlation treatment, which automatically includes also the local spin and charge fluctuation effects. As can be seen, CMRT gives comparable equilibrium volume and bulk modulus as LDA+DMFT. While having different physical and computational philosophy considerations behind, CMRT and LDA+DMFT agree very well on the change of energy as a function of volume, which might validate use of the specific values of the volume-dependent effective U_f in the Refs. [3,39]. Taking the inferred experimental energy curve as reference, we cannot tell which method performs the best among SIC-LSDA, CMRT, and LDA+DMFT.

The pressure verses volume (P-V) curves should pose as a more stringent validity check on the total-energy calculation as pressure is the first-order derivative of energy with respect to volume and meanwhile pressure is directly accessible from experiments. The fitted P-V curves on fcc Pr from the above-mentioned methods are presented in Fig. 2

TABLE I. Calculated equilibrium volume V_{eq} and bulk modulus B_0 of fcc Pr in comparison with experimental measurements as well as other methods. Relevant data are derived or cited from LDA [15], Expt [15], SIC-LSDA [36], and LDA+DMFT [39] (abbreviated as DMFT).

	Expt(dhcp)	LDA	GGA	SIC-LSDA	DMFT	CMRT
V_{eq} (Å^3)	34.54	21.01	24.03	31.84	34.64	35.13
B_0 (GPa)	26–37	59.47	38.70	29.08	31.32	23.71

and compared directly against experimental measurements on a set of Pr crystal phases. The agreement between CMRT and LDA+DMFT [39] and between CMRT and experiments [3,48] nearby the fcc and dfcc phases are exceptionally good. On the other hand, the pressure behavior out of SIC-LSDA shows marked deviation from the fcc and dfcc phases, although it is already quite good for a qualitative description. The volume-collapse transition between the dfcc and α-U phases is not explicitly investigated in this study because further CMRT development is still needed to better handle the calculation for the latter phase. But surprisingly, NLCF of $4f$ electrons evaluated within the fcc phase signals a sharp turn right within the narrow volume range bracketing the volume-collapse transition across the two different phases. This sharp turn in NLCF calculated with local $4f$ electrons in fcc Pr reflects qualitative change in the nature of electronic correlation of the local $4f$ electron and its localization status across some threshold volume. Without looking into α-U phase in this study, we are still able to glean some physical origin of the volume-collapse phase transition. This seemingly controversial fact might actually reflect the local nature of the correlated $4f$ electrons and their minor role played in participating in the directional bonding forming a specific lattice, thus rendering NLCF a physical quantity insensitive to environment. The consistency between NLCF and the volume collapse transition is also seen in Ce [22]. The possible connection between the correlated $4f$ electrons and the localization physics reflected in NLCF will be elaborated in a future publication.

B. Onsite f occupational probability comparisons among different methods and against experiments

Local correlated Fock state occupational probability p_Γ is the next set of physical quantities directly accessible in CMRT through defining the exact local onsite energy of the correlated $4f$ electrons in terms of p_Γ. By grouping the Fock states in the $4f$ subspace into disjoint subsets f^n, with n being the number of electrons filling a Fock state, the onsite f occupational probability W_f equals the sum of p_Γ over all Fock states in a given subset. Experimentally, however, W_f is only indirectly obtained through, say, x-ray absorption experiments [49]. W_f is meaningful in that it provides a unique way to look into a theoretical description of correlation effects at the multi-electron wave function level. Its value cannot be correctly produced in static mean-field methods like DFT without exploiting special tricks setting electronic occupation [50] but comes out readily with CMRT. Given a set of slowly varying orbital occupation of quasiparticles, W_f in the noninteracting limit can be shown to be nearly featureless across a certain volume range, while its interacting counterpart can have more pronounced features as volume or pressure varies [15]. These pronounced features are also observed in CMRT, as shown in Fig. 3. Figure 3(a) gives a comparison of W_{f^3}/W_{f^2}, the dominant two components of W_f of fcc Pr, among CMRT, LDA+DMFT, and experiments and attests to the qualitative agreement among these different approaches. Figure 3(b) presents the pressure dependence of W_f in each dominant subset of Fock states between CMRT and LDA+DMFT [41]. Both the trends of W_f and the signature crossing between f^2 and f^3 reported in LDA+DMFT are reasonably well reproduced in CMRT. Figure 3(c) compares total $4f$ electron occupation n_f between CMRT and LDA+DMFT as well as pressure dependence of renormalization prefactor of local $4f$ orbits, z_f, obtained with CMRT. The overall agreement on n_f between the two methods are more or less consistent with the deviation of W_f in Fig. 3(b). The correlation strength reflected with z_f is also consistent with the expected behavior of $4f$ electron correlation with increasing volume. Considering that the two methods utilize different choices for local orbital construction and disparate self-consistent formulation framework to solve two seemingly different correlated Hamiltonians yet describing roughly the same physical problem, the nice overall agreement of the dominant features of W_f and energy-volume curves between CMRT and LDA+DMFT on fcc Pr should not be considered simply as a coincidence but suggests that the essential strong correlation physics were captured by both theories although their formalism and frameworks are different.

IV. DISCUSSION

A quick comparison on different energy parameters might be helpful in giving one an overview on the typical magnitudes of different Coulomb interactions in fcc Pr. We compiled volume dependence of bare local direct Coulomb interaction coefficients, $U_{iiii}^{\alpha\beta\alpha\beta}$ defined in Eq. (2), within the same and between different $4f$ orbits, and bare nearest (nn) and next-nearest (nnn) neighboring $U_{ijij}^{\alpha\beta\alpha\beta}$ for $i \neq j$ in Fig. 4. These data are averaged over $4f$ orbits to simplify their display. The

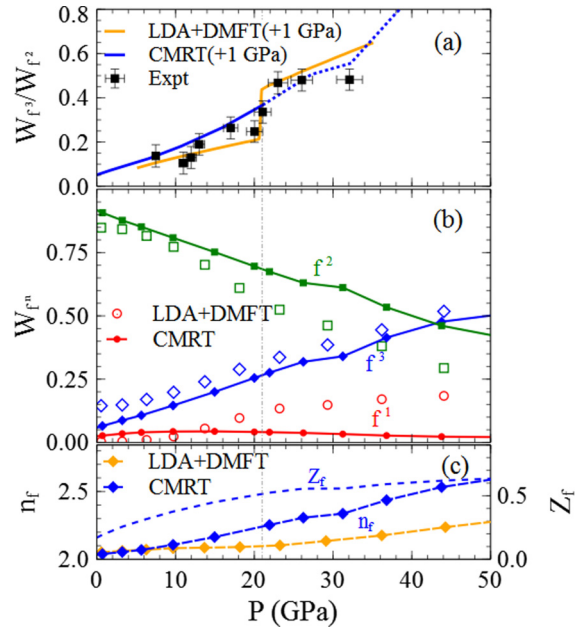

FIG. 3. Panel (a) shows pressure dependence of W_{f^3}/W_{f^2} for CMRT, LDA+DMFT (U_f volume dependent, $T = 632$ K, with SOI) [41] evaluated on fcc Pr and experimental measurements [49]. A shift of $+1$ GPa is applied to the calculations in accordance with Fig. 3 in Ref. [49]. CMRT data are shown in blue with a solid line at low pressure and with a dotted line at high pressure separated by the experimental fcc–α-U phase boundary. Same information for LDA+DMFT is shown in orange. Panel (b) presents pressure dependence of W_{f^n} from CMRT in filled symbols and LDA+DMFT in empty symbols. Different colors denote $n = 1, 2, 3$, respectively. Panel (c) presents pressure dependence of renormalization prefactors of $4f$ orbits from CMRT, shown as a dashed line and referring to the right vertical axis, and total $4f$ electron occupation from both CMRT and LDA+DMFT [39], shown as a line + symbol and referring to the left vertical axis. Renormalization prefactors are averaged over $4f$ orbits to make the presentation less cumbersome.

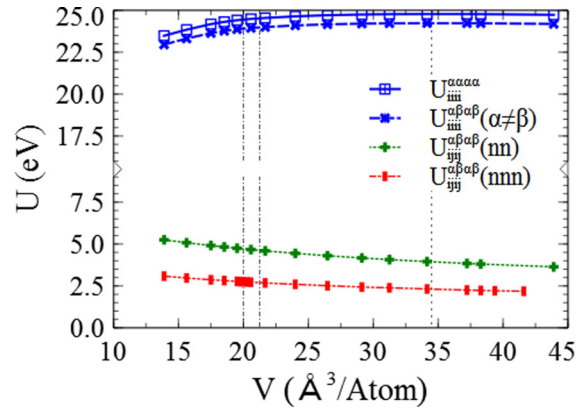

FIG. 4. Volume dependence of bare local direct Coulomb interaction coefficients within and between orbits, $U_{iiii}^{\alpha\beta\alpha\beta}$, as well as between the nearest and next-nearest neighboring sites, $U_{ijij}^{\alpha\beta\alpha\beta}(nn)$ and $U_{ijij}^{\alpha\beta\alpha\beta}(nnn)$. These quantities are averaged across the correlated $4f$ orbits to simplify display. Note the broken y axis to show details of the curves.

screened local Hubbard interaction, U_f of $4f$ orbits for fcc Pr, is around 7 eV with a weak volume dependence [3]. The much smaller magnitude of U_f as compared against $U_{iiii}^{\alpha\beta\alpha\beta}$ is interpreted to be due to electronic screening effects from itinerant electrons out of $4f$ orbits [16]. Such a reduction in electronic correlation is utilized to help formulate the DFT embedding theories to work toward strongly correlated systems. The bare intersite $U_{ijij}^{\alpha\beta\alpha\beta}$ follows the inverse distance Coulomb decaying behavior and its nearest neighboring value has a magnitude comparable to U_f. Since these terms are left untreated in GA due to the infinite dimension limit and can bring up considerable error in total-energy evaluation, they have to be corrected for a practically useful theory. Our way to help with that is to introduce the sum-rule coefficient λ_i^α, which is actually a weighted nonlocal bare direct Coulomb interaction slightly smaller than $U_{ijij}^{\alpha\beta\alpha\beta}(nnn)$ in fcc Pr due to fast decay of hopping in its definition. Another feature one might observe from the figure is that these energy parameters are quite flat throughout the volume range, reflecting the local nature of the $4f$ orbits and their weak participation in bonding formation of the Pr lattice. Such a feature is consistently verified in other physical quantities studied here, like NLCF.

The existing theoretical exploration on Pr reveals equivocal views on the relevant physical mechanisms underlying the experimental measurements, whether it has phase sensitivity, many body effects, or a delicate competition among them. A spin-polarized GGA calculation assuming $4f$ band electrons [31] performed better in total-energy calculations than a very similar calculation using the standard model of RE treating $4f$ electrons as core electrons [29]. This seems to indicate many body effects leading to localization play a minor role on Pr. Meanwhile, LDA+DMFT [39–41] in a paramagnetic ground state were able to produce a broad range of physical quantities consistent with experiments. The complicated correlation effects played out of the many-body interactions seem to say that a spin-polarized ground state is a nonessential ingredient for dominant physical properties of Pr, but the existence of local moment and the local correlation physics producing it is more relevant. Taking the fact that LDA+DMFT accounts for many physical facts and is the best calculation so far on Pr, we thus chose to work with a paramagnetic state in CMRT to have a fair comparison with LDA+DMFT and consider correlation effects on how electronic behavior might be affected with volume change. Figure 3 strongly suggests CMRT also comes with local moment in its paramagnetic ground state, just like LDA+DMFT.

While good agreement (see Figs. 1 and 2) gives us quite some confidence in the overall validity and practicality of CMRT, we stress that temperature and SOI effects were not included in the current calculation. We understand that these effects can be significant on the details of observed phenomena in the rare-earth compounds, but on this stage, we hope the energy scale of these physical effects is smaller than the electronic correlation energy range. On the other hand, the experimental energy curve given in Fig. 1 was obtained through postprocessing of data measured at different temperatures and assumed to fulfill certain requirements [39,48]. Thus, comparisons against experiments should be carried out with caution if the condition and accuracy of the relevant results were hard to determine. For example, taking the experimental energy curve as the reference in Fig. 1, SIC-LSDA, CMRT and LDA+DMFT results should be thought of as being equally good in their performance. Figure 2 further tells which result among them performs better.

We might ask a further question on what determines a feasible theory to describe Pr systems. Unlike fcc Ce and its isostructural volume collapse transition, which is hard to reproduce in a theory, quite a few *ab initio* methods have claimed to qualitatively reproduce the volume collapse in Pr [15,31,36,39,51]. The equilibrium volume and bulk modulus were also quite successfully described [40]. Thus, the P-V curve is a more stringent criterion than the E-V curve to judge the quality of a theoretical description on Pr. SIC-LSDA and LDA+DMFT produced the best description of P-V curves so far. However, they dealt with different degrees of Coulomb correlations and corrected different aspects of DFT. Thus their successes became quite confusing in revealing the role of electronic correlation as well as the most influential technical concerns. CMRT avoids all the unnecessary complications: it does not have self-interaction by its theoretical design, copes directly with the real Coulomb interactions, gives the expected trivalent state out of correlation, and self-adjusts screening through Gutzwiller renormalization prefactors and local electronic configuration occupations, not to mention it still maintains the convenience of DFT formalism. As long as the physics inherent in the Pr systems does not exceed the description of the current Gutzwiller trial wave function, CMRT might be a very suitable tool for the Pr systems. Back towards the question of what makes a trustworthy theory for Pr: It has to reproduce all the major physical measurements instead of a selected few of what are usually supposed to be significant.

CMRT is by design capable of giving as much electronic structure information as DFT, but more work is needed at the moment to generate an accurate quasiparticle spectrum to check against experimental XPS and BIS spectroscopy. Some pure theoretical inferences might still be made by comparing the currently available electronic structures across similar phases of Ce and Pr, both sharing very similar physical properties and effective Hubbard parameters [3]. Specifically, Pr has a larger DOS at E_f than Ce in the CMRT calculation, which might indicate that Pr is closer to a magnetic instability than Ce based on the Stoner mechanism [52]. Thus more eminent local moment or even a spontaneous magnetic phase transition is expected from Pr, which is consistent with experiments that fcc Pr has a small ordered magnetic moment and a low Curie temperature of 8.7 K while fcc Ce is paramagnetic [53,54].

V. SUMMARY

In this work, we have applied CMRT, a fully *ab initio* method for correlated electron materials, on fcc Pr to study the volume dependence of total energy of a paramagnetic ground state starting from the bare lattice Hamiltonian without any adjustable energy parameters. We showed that CMRT produced a pressure volume curve in decent agreement with experiments and generated consistent results with LDA+DMFT. We also presented volume dependence of normalized local charge fluctuation (NLCF) of $4f$ electrons [22] and showed that its maximum aligns well with the volume

collapse region of Pr. This is interpreted to be a signature of a localization-delocalization transition around the dfcc to the α-U phase transition in Pr. In comparison with LDA+DMFT, CMRT is option-free from choices of effective U and J parameters and double-counting terms. It would thus be an appropriate tool for a strongly correlated electron calculation if DFT embedding methods are too sensitive to those choices. Since the computational speed of CMRT is similar to that of minimal basis HF calculations and computationally much faster, it is a good approach in case only limited computational resource is available. In addition, while LDA+DMFT using QMC as its impurity solver would have a stochastic nature and thus limited accuracy in a total-energy calculation (currently 0.01 eV or so), CMRT is a deterministic theory and does not have such a limitation.

ACKNOWLEDGMENTS

This work was supported by the U.S. Department of Energy (DOE), Office of Science, Basic Energy Sciences, Materials Science and Engineering Division, including the computer time support from the National Energy Research Scientific Computing Center (NERSC) in Berkeley, California. The research was performed at Ames Laboratory, which is operated for the U.S. DOE by Iowa State University under Contract No. DEAC02-07CH11358.

[1] P. Hohenberg and W. Kohn, Phys. Rev. **136**, B864 (1964).
[2] W. Kohn and L. J. Sham, Phys. Rev. **140**, A1133 (1965).
[3] A. K. McMahan, C. Huscroft, R. T. Scalettar, and E. L. Pollock, J. Comput.-Aided Mater. Des. **5**, 131 (1998).
[4] L. Shulenburger and T. R. Mattsson, Phys. Rev. B **88**, 245117 (2013).
[5] M. Motta, D. M. Ceperley, G. K.-L. Chan, J. A. Gomez, E. Gull, S. Guo, C. A. Jiménez-Hoyos, T. N. Lan, J. Li, F. Ma, A. J. Millis, N. V. Prokof'ev, U. Ray, G. E. Scuseria, S. Sorella, E. M. Stoudenmire, Q. Sun, I. S. Tupitsyn, S. R. White, D. Zgid, and S. Zhang (Simons Collaboration on the Many-Electron Problem), Phys. Rev. X **7**, 031059 (2017).
[6] U. Schollwöck, Rev. Mod. Phys. **77**, 259 (2005).
[7] E. M. Stoudenmire, L. O. Wagner, S. R. White, and K. Burke, Phys. Rev. Lett. **109**, 056402 (2012).
[8] Z.-H. Cui, T. Zhu, and G. K.-L. Chan, J. Chem. Theory Comput. **16**, 119 (2020).
[9] T. Zhu, Z.-H. Cui, and G. K.-L. Chan, J. Chem. Theory Comput. **16**, 141 (2020).
[10] F. Nilsson and F. Aryasetiawan, Computation **6**, 26 (2018).
[11] V. I. Anisimov, J. Zaanen, and O. K. Andersen, Phys. Rev. B **44**, 943 (1991).
[12] G. Kotliar, S. Y. Savrasov, K. Haule, V. S. Oudovenko, O. Parcollet, and C. A. Marianetti, Rev. Mod. Phys. **78**, 865 (2006).
[13] X. Y. Deng, L. Wang, X. Dai, and Z. Fang, Phys. Rev. B **79**, 075114 (2009).
[14] K. M. Ho, J. Schmalian, and C. Z. Wang, Phys. Rev. B **77**, 073101 (2008).
[15] N. Lanatà, Y. Yao, C.-Z. Wang, K.-M. Ho, and G. Kotliar, Phys. Rev. X **5**, 011008 (2015).
[16] F. Aryasetiawan, K. Karlsson, O. Jepsen, and U. Schönberger, Phys. Rev. B **74**, 125106 (2006).
[17] S. Ryee and M. J. Han, Sci. Rep. **8**, 9559 (2018).
[18] M. Karolak, G. Ulm, T. Wehling, V. Mazurenko, A. Poteryaev, and A. Lichtenstein, J. Electron Spectrosc. Relat. Phenom. **181**, 11 (2010).
[19] Y. X. Yao, J. Liu, C. Z. Wang, and K. M. Ho, Phys. Rev. B **89**, 045131 (2014).
[20] X. Zhao, J. Liu, Y.-X. Yao, C.-Z. Wang, and K.-M. Ho, Phys. Rev. B **97**, 075142 (2018).
[21] J. Liu, X. Zhao, Y. Yao, C.-Z. Wang, and K.-M. Ho, J. Phys.: Condens. Matter **33**, 095902 (2021).
[22] J. Liu, Y. Yao, J. Zhang, K.-M. Ho, and C.-Z. Wang, Phys. Rev. B **104**, L081113 (2021).
[23] B. Johansson, Phys. Rev. B **20**, 1315 (1979).
[24] Y. C. Zhao, F. Porsch, and W. B. Holzapfel, Phys. Rev. B **52**, 134 (1995).
[25] S. R. Evans, I. Loa, L. F. Lundegaard, and M. I. McMahon, Phys. Rev. B **80**, 134105 (2009).
[26] J. K. Lang, Y. Baer, and P. A. Cox, Phys. Rev. Lett. **42**, 74 (1979).
[27] J. K. Lang, Y. Baer, and P. A. Cox, J. Phys. F: Met. Phys. **11**, 121 (1981).
[28] H. W. Myron and S. H. Liu, Phys. Rev. B **1**, 2414 (1970).
[29] P. Söderlind, P. E. A. Turchi, A. Landa, and V. Lordi, J. Phys.: Condens. Matter **26**, 416001 (2014).
[30] W. M. Temmerman, Z. Szotek, and H. Winter, Phys. Rev. B **47**, 1184 (1993).
[31] P. Söderlind, Phys. Rev. B **65**, 115105 (2002).
[32] A. Delin, L. Fast, B. Johansson, O. Eriksson, and J. M. Wills, Phys. Rev. B **58**, 4345 (1998).
[33] B. Min, H. Jansen, T. Oguchi, and A. Freeman, J. Magn. Magn. Mater. **59**, 277 (1986).
[34] O. Eriksson, M. S. S. Brooks, and B. Johansson, Phys. Rev. B **41**, 7311 (1990).
[35] J. P. Perdew and A. Zunger, Phys. Rev. B **23**, 5048 (1981).
[36] A. Svane, J. Trygg, B. Johansson, and O. Eriksson, Phys. Rev. B **56**, 7143 (1997).
[37] Z. Szotek, W. Temmerman, and H. Winter, Phys. B (Amsterdam, Neth.) **172**, 19 (1991).
[38] M. Casadei, Ph.D. thesis, der Freie Universitat Berlin, 2013 (unpublished).
[39] A. K. McMahan, Phys. Rev. B **72**, 115125 (2005).
[40] I. L. M. Locht, Y. O. Kvashnin, D. C. M. Rodrigues, M. Pereiro, A. Bergman, L. Bergqvist, A. I. Lichtenstein, M. I. Katsnelson, A. Delin, A. B. Klautau, B. Johansson, I. Di Marco, and O. Eriksson, Phys. Rev. B **94**, 085137 (2016).
[41] A. K. McMahan, R. T. Scalettar, and M. Jarrell, Phys. Rev. B **80**, 235105 (2009).
[42] C. Liu, J. Liu, Y. X. Yao, P. Wu, C. Z. Wang, and K. M. Ho, J. Chem. Theory Comput. **12**, 4806 (2016).
[43] J. Bünemann, F. Gebhard, and W. Weber, J. Phys.: Condens. Matter **9**, 7343 (1997).
[44] M. Fabrizio, Phys. Rev. B **76**, 165110 (2007).
[45] G. Kresse and J. Furthmüller, Phys. Rev. B **54**, 11169 (1996).

[46] X. Qian, J. Li, L. Qi, C.-Z. Wang, T.-L. Chan, Y.-X. Yao, K.-M. Ho, and S. Yip, Phys. Rev. B **78**, 245112 (2008).
[47] F. D. Murnaghan, Proc. Natl. Acad. Sci. USA **30**, 244 (1944).
[48] B. J. Baer, H. Cynn, V. Iota, C.-S. Yoo, and G. Shen, Phys. Rev. B **67**, 134115 (2003).
[49] J. A. Bradley, K. T. Moore, M. J. Lipp, B. A. Mattern, J. I. Pacold, G. T. Seidler, P. Chow, E. Rod, Y. Xiao, and W. J. Evans, Phys. Rev. B **85**, 100102 (2012).
[50] P. Söderlind, A. Landa, J. Tobin, P. Allen, S. Medling, C. Booth, E. Bauer, J. Cooley, D. Sokaras, T.-C. Weng, and D. Nordlund, J. Electron Spectrosc. Relat. Phenom. **207**, 14 (2016).
[51] E. Arola, M. Horne, P. Strange, H. Winter, Z. Szotek, and W. M. Temmerman, Phys. Rev. B **70**, 235127 (2004).
[52] S. H. Simon, *The Oxford Solid State Basics*, 1st ed. (Oxford University Press, Oxford, UK, 2013).
[53] A. V. Nikolaev and A. V. Tsvyashchenko, Phys. Usp. **55**, 657 (2012).
[54] E. Bucher, C. W. Chu, J. P. Maita, K. Andres, A. S. Cooper, E. Buehler, and K. Nassau, Phys. Rev. Lett. **22**, 1260 (1969).